Research Article | Vol. 31, No. 12 / 5 Jun 2023 / Optics Express 19843
Optics EXPRESS

Stadium-type resonator sensor based on a multi-mode waveguide with mode discrimination phenomenon

JAE-SANG LEE, YONG-JIN KIM, SEONG-HYEON CHO, BYEONG-TAK PARK, WOO JUNE CHOI, AND YOUNG-WAN CHOI*

Advanced Photonics Laboratory, Department of Electrical and Electronics Engineering, Chung-Ang University, Seoul, 06974, Republic of Korea
*ychoi@cau.ac.kr

Abstract: In this work, we present a multi-mode resonator based on SU-8 polymer and experimentally verify that the resonator showed mode discrimination can be used as a sensor with high performance. According to field emission scanning electron microscopy (FE-SEM) images, the fabricated resonator shows sidewall roughness which is canonically considered to be undesirable after a typical development process. In order to analyze the effect of sidewall roughness, we conduct the resonator simulation considering the roughness under various conditions. Mode discrimination still occurs even in the presence of sidewall roughness. In addition, waveguide width controllable by UV exposure time effectively contributes to mode discrimination. To verify the resonator as a sensor, we perform a temperature variation experiment, which results in a high sensitivity of about 630.8 nm/RIU. This result shows that the multi-mode resonator sensor fabricated via a simple process is competitive with other single-mode waveguide sensors.

1. Introduction

Biochemical sensors have gained increasing attention in medical healthcare [1–6], and the COVID-19 pandemic has further accelerated research in this area [7]. Optical resonators have attracted significant interest among various sensors due to their high sensitivity and label-free methodology [8–11]. The changes in the refractive index of the environment can be detected by measuring the shifts of the peak wavelength of the resonator. Currently, most optical resonators are based on a nano-scale single-mode waveguide which offers advantages such as low modal dispersion and high sensitivity [9,10]. However, the single-mode resonator is vulnerable to fabrication errors. For example, in a ring resonator, even a slight error in a gap between the bus waveguide and the ring can significantly affect the coupling ratio and transmission spectra [12]. Thus, nano-scale resonators require much attention for mass production, so a relatively high-cost fabrication must be employed.

In order to develop a sensor that can be mass-produced and is insensitive to fabrication errors, we proposed a multi-mode resonator that exhibits the mode discrimination phenomenon [12,13]. Mode discrimination refers to removing the higher-order modes thanks to the loss difference between the higher-order modes and the fundamental-mode [14,15]. This results in a transmission spectrum that resembles that of a single-mode-based resonator. As a multi-mode waveguide-based resonator, a relatively simple and straightforward process can be employed, making mass production easily achievable.

In this paper, we demonstrate the multi-mode waveguide-based resonator as a temperature sensor. To validate this resonator as a sensor, we fabricate a stadium-type resonator based on SU-8 polymer using a simple photolithography process. The resonator images are captured by field emission scanning electron microscopy (FE-SEM). However, fabricated devices show a sidewall

#489554 https://doi.org/10.1364/OE.489554
Journal © 2023 Received 10 Mar 2023; revised 2 May 2023; accepted 18 May 2023; published 30 May 2023

Optics EXPRESS

roughness that occurred during the development step. To analyze its effect, we design a waveguide segment with varying widths to account for the sidewall roughness and stacked them together for the simulation. We analyze the simulation results and compare them with the experimental results. Sidewall roughness causes additional loss in particularly higher-order modes and results in the acceleration of mode discrimination. Moreover, mode discrimination is affected not only by sidewall roughness but also by the waveguide width, which can be adjusted by controlling UV exposure time in the fabrication process. As waveguide width is one of the crucial factors determining the confinement factor of the guided modes and the loss in a waveguide, we analyze the effect of waveguide width on mode discrimination based on simulation and experiments. As a result, mode discrimination occurs more effectively as the width of the waveguide decreases. In order to validate the proposed device as a sensor, we conduct a temperature variation experiment. The sensitivity of the device is comparable to other single-mode waveguide-based resonators. Therefore, the proposed sensor provides high performance similar to that of the single-mode resonators, although the device itself is multi-mode, thanks to the mode discrimination obtained from the special design of the sensor. In addition, it is insensitive to fabrication errors, which makes it suitable for mass production.

2. Design and fabrication of the multi-mode waveguide-based resonator

2.1. Design of resonator based on multi-mode waveguide

We designed a multi-mode waveguide based multi-mode interference (MMI) coupler and resonator, as shown in Fig. 1. We reported a multi-mode waveguide-based resonator with mode discrimination [12]. MMI width and length were designed for a 50:50 division ratio to minimize the back reflection, and the radius in the bending structure is determined to be 9 µm which has enough loss difference between the fundamental-mode and higher-order modes to induce mode discrimination. Bending loss (α) is determined concerning the effective refractive index, as expressed in Eq. (1) [16]. The value of K is determined by the refractive index of the core, cladding, and height of the waveguide, and Δn_{eff} is the index difference between cladding and core effective index (n_{eff}). Since the effective index is proportional to the propagation constant (β), the bending loss of the fundamental mode is smaller than that of the higher-order modes. Therefore, higher-order modes are rapidly reduced as light propagates through the bending structure. The stadium shape resonator is shown in Fig. 1 (b), and the total length of the resonator is about 713 µm.

$$\alpha = K \cdot \exp(-cR), \quad c = \beta \cdot \left(\frac{2 \cdot \Delta n_{eff}}{n_{eff}}\right)^{\frac{3}{2}} \tag{1}$$

2.2. Fabrication recipe and results

We chose SU-8 as the constituent material for the resonator because of its negligible optical absorption in the wavelength near 1550 nm and its ease of fabrication in producing waveguides [17,18]. Additionally, the compatibility of SU-8 with the photolithography process makes it suitable for mass production. The resonator is fabricated on a silicon-on-insulator (SOI) wafer (thickness 500 ± 25 µm) with a 14.5 µm thickness of oxide film. A 4-inch SOI wafer is cleaved into rectangular (1.5 cm × 1.5 cm) specimens. The specimen is cleaned, dried, and baked as the first process. Hexamethyldisilane (HMDS) is spin-coated to the substrate and baked (120 °C, 1 min) to increase the adhesion of SU-8 2002. After that, SU-8 2002 is spin-coated for a height of 2.18 µm. Removing the edge bead formed on the edge of the rectangular wafer to minimize a gap between a mask and spin-coated wafer, the substrate is soft-baked (95 °C, 2 min) and exposed (10 sec, 17 J/cm) to UV light (I-line, 365 nm). For the last step, post-exposure bake (95 °C, 2 min) and development are conducted to complete the fabrication process. Only a single photolithography process is required as described. The resonator's top and top-front views are

Optics EXPRESS

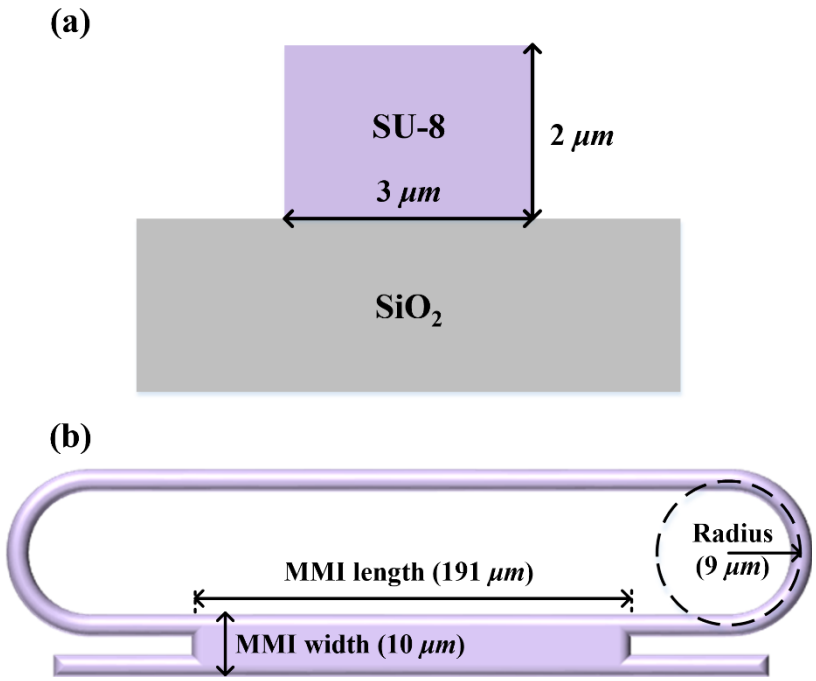

Fig. 1. (a) Cross-section of the multi-mode waveguide, (b) design parameter and the structure of stadium shape resonator with MMI coupler.

shown in Fig. 2(a, b) using FE-SEM. It is observed that the structure had sidewall roughness throughout, as shown in Fig. 2(b). The shape of the fabricated waveguide is not rectangular, but rather trapezoidal, due to the thermal reflow that occurs during the fabrication process. The sidewall angle of the waveguide affects the resonator, including mode confinement and MMI coupling ratio, accelerating mode discrimination [13].

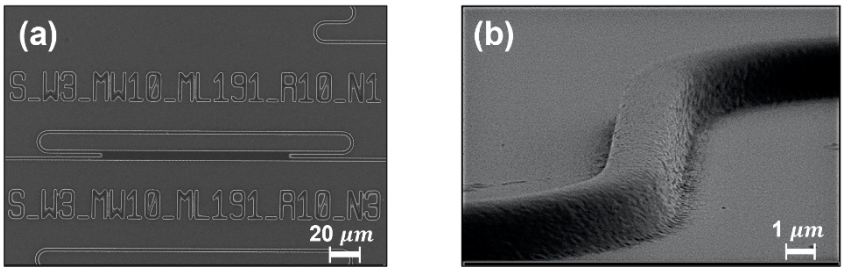

Fig. 2. Field emission scanning electron microscopy (FE-SEM) image of the fabricated device (a): top view and (b): top-front view of bending structure in the resonator.

3. Analysis of the effect of sidewall roughness

3.1. Design of bending structure with sidewall roughness

Sidewall roughness at the interface between SU-8 and air causes a change in total internal reflection, leading to a change in the transmission spectrum. To analyze the effect of roughness, we conduct a simulation using the MODE solution based on the finite-difference time-domain

Optics EXPRESS

method. To simulate a waveguide with sidewall roughness, we design various waveguide fragments, where the width of each fragment waveguide is a combination of a 3 μm width and a random variable(W_r) less than the maximum roughness width ($W_{r,max}$), as shown in Fig. 3. These fragment waveguides were stacked at 0.5° degree intervals as depicted in Fig. 4. By following this procedure, the bending structure for simulation becomes similar to the fabricated structure as illustrated in Fig. 2(b). Through this simulation, we analyze the impact of the sidewall roughness on the mode discrimination.

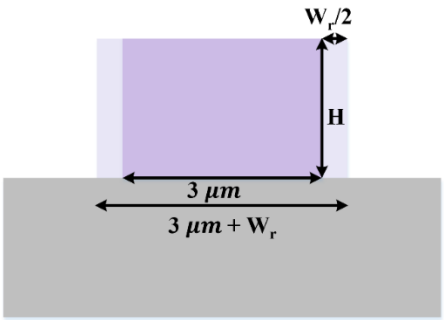

Fig. 3. Designed waveguide with random variable to apply the sidewall roughness. Based on the FE-SEM image, base widths are 3 μm, and the range of sidewall roughness (W_r) is an arbitrary value within the range of maximum roughness width ($W_{r,max}$).

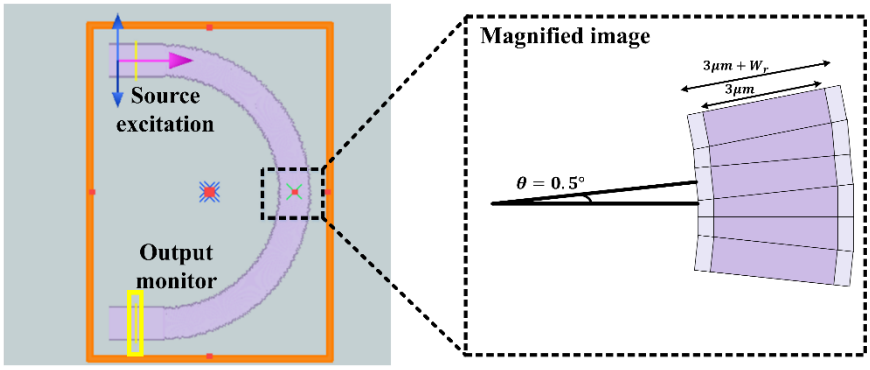

Fig. 4. Designed bending structure with sidewall roughness. Each fragment waveguide is stacked at 0.5° intervals to simulate the waveguide with a sidewall roughness.

3.2. *Effect of sidewall roughness on mode discrimination*

Figure 5 shows the simulation results of each mode loss with respect to the sidewall roughness. It is evident that overall losses tend to increase along with the sidewall roughness. Data that deviate from the constantly increasing characteristic appear to be errors resulting from the irregular characteristics of the segments set in the simulation. Irregularity can arise due to the random variable width (W_r) within $W_{r,max}$. In addition, the stacking process is performed discretely, which may lead to discontinuous parts, resulting in slight errors in Fig. 5. However, it is evident that the tendency for loss changes remains. The losses of the higher-order modes (TE1, TM1) increase significantly compared to the losses of the fundamental-mode (TE0, TM0) as the sidewall roughness increases. Thus, the intensities of the higher-order modes are suppressed, while that of the fundamental-mode decreases relatively slowly. Sidewall roughness, which may

Optics EXPRESS

canonically be considered as a fabrication error, interestingly contributes positively towards mode discrimination. Therefore, two bending structures in the stadium-type resonator sufficiently reduce the higher-order modes and preserve only the fundamental-mode.

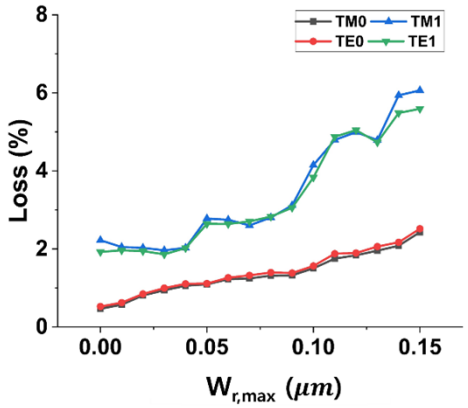

Fig. 5. Effect of the sidewall roughness on the propagation loss of each mode passing through the bending structure. $W_{r,max}$ is the maximum value of the random variable W_r.

4. Experimental results and discussion

4.1. Experimental setup

We established an experimental setup to validate the multi-mode waveguide-based resonator as a sensor, as depicted in Fig. 6. The source stage comprises a super-luminescent light-emitting diode (DL-CS5203A, Dense Light Semiconductors) and a laser diode controller (LDC-3724C, Newport). The input source is coupled to the device stage using a single-mode lensed fiber to minimize coupling loss between the source and the resonator. Generally, using a lensed fiber is a convenient way to enhance the coupling efficiency between optical fibers and waveguides. A piezo actuator enables precise control of the input and output fiber positions for accurate alignment. The transmitted light through the output fiber is measured using an optical spectrum analyzer (MS9740A, Anritsu). A Peltier device is mounted beneath the resonator and controlled using a thermoelectric cooler (LDC-3722B, Anritsu). We set the initial temperature to 20 °C and allowed it to stabilize for at least 10 minutes to maintain a stable temperature.

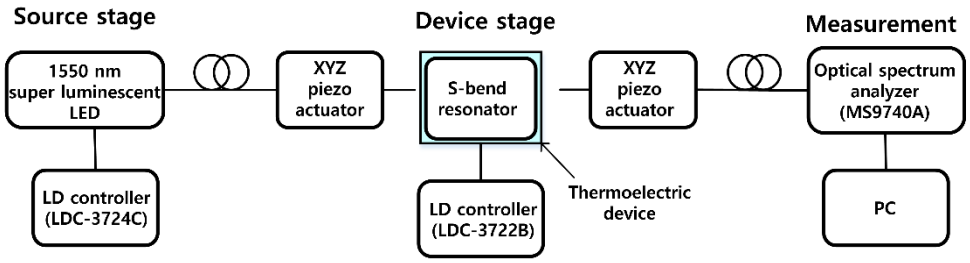

Fig. 6. Schematic of an experimental setup.

4.2. Analysis of the waveguide width and sidewall roughness effects

Figure 7 shows the measured transmission spectra of two different resonators, one based on a 3.2 µm width waveguide (Fig. 7(a)) and the other based on a 3 µm width waveguide (Fig. 7(b)).

Optics EXPRESS

The transmission spectrum of the 3.2 μm width resonators exhibits multi-peaks, but multi-peaks in the 3 μm width resonance spectrum are almost removed and increased the extinction ratio. Therefore, the 3.2 μm width resonator has limited as a sensor, whereas a resonator with a 3 μm width resonator can be utilized as a sensor. The reason for the different results is that the waveguide width is a crucial factor in determining the mode confinement. Figure 8 illustrates the mode profile and confinement factor of the 3 μm and 3.2 μm width waveguide. The wider waveguide has a higher overall confinement factor, which means that the modes in wider waveguide are confined better. Notably, the TE4 mode is confined in the 3.2 μm waveguide but not in the 3 μm waveguide. As depicted in Fig. 9, the waveguide width can be adjusted by varying the UV exposure time. This is because SU-8 is a negative-type photoresist, and increasing the UV exposure time leads to a larger irradiated volume of the photoresist, resulting in a slight increase in the waveguide width. The exposure times for the waveguides with widths of 2.32, 2.71, 3.00, and 3.20 μm were 6, 8, 10, and 12 seconds, respectively. Hence, precise control of the UV exposure time can enhance the efficiency of mode discrimination.

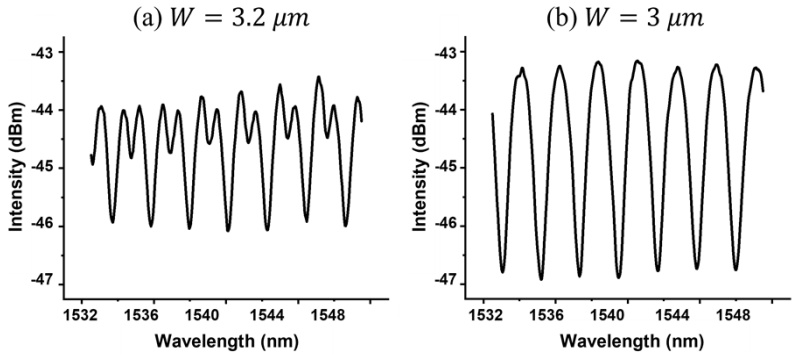

Fig. 7. Transmission spectra of the multi-mode waveguide-based resonator. Spectrum in (a) was shown multi-peaks and a reduced extinction ratio, and that in (b) was shown a reduction of multi-peaks and increased extinction ratio.

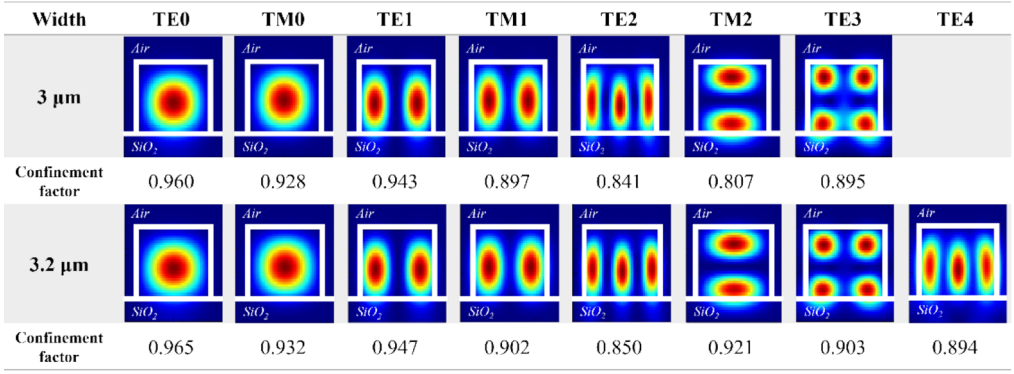

Fig. 8. Mode profile of both cases that waveguide width is 3 μm and 3.2 μm width. The number of modes is increased according to waveguide width. The white box indicates the waveguide based on SU-8.

In order to analyze the resonance characteristic according to the waveguide width and sidewall roughness, we simulate the 3 μm and 3.2 μm width resonator with varying levels of sidewall roughness, as shown in Fig. 10 and Fig. 11. Both simulations reveal that the higher-order mode's

Optics EXPRESS

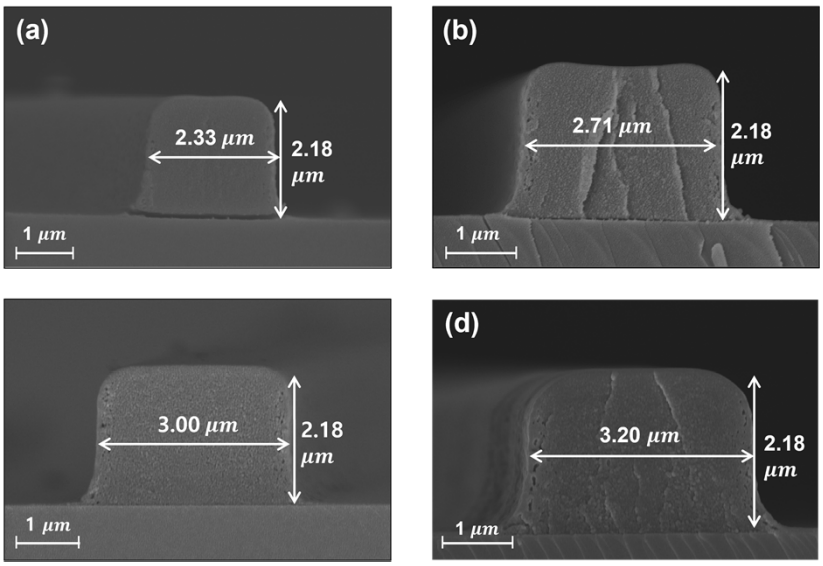

Fig. 9. Cross-sectional FE-SEM images of the fabricated waveguide with different UV exposure times (a) 6 sec, (b) 8 sec, (c) 10 sec. and (d) 12 sec.

propagation loss increases as sidewall roughness increases, leading to a reduction of multi-peaks in the spectra as the influence of the fundamental mode becomes more dominant. The overall intensity of the transmission spectra in Fig. 10(a) and Fig. 11(a) is larger than Fig. 10(b-d) and Fig. 11(b-d) as it represents the superposition of the fundamental and higher-order modes transmission spectra. Comparing Fig. 10 with Fig. 11 to analyze the effect of waveguide width on the resonator, the 3.2 µm width resonator has more multi-peaks in its spectrum than the 3 µm width resonator due to the considerable influence of higher-order modes.

4.3. Experimental validation as a sensor

We perform a temperature variation experiment to validate the fabricated device as a sensor. The stage is combined with a thermoelectric cooler and maintained for more than 10 minutes to ensure sufficient heat transfer to the device. We varied the temperature from 20 °C to 30 °C at intervals of 2 °C and observed a shift in the resonance spectrum, as shown in Fig. 12. The FSR, FWHM, and Q-factor of the device is 2.16 nm, 1.55 nm, and about 10^3, respectively. The average resonance shift is 82 pm/°C, and the extinction ratio is approximately 3.5 dB, which is considered sufficient for the sensor use. The sensitivity of the resonator is 82 pm/°C for temperature sensing and 630.8 nm/RIU for biosensing which is calculated by taking the reciprocal of the SU-8's thermos-optic coefficient (-1.3×10^{-4} C^{-1}) [19] and multiplying it by the measured wavelength shift. On the other hand, SU-8 has a coefficient of thermal expansion of 52 ppm/°C, so for a temperature change of 10°C, the change in waveguide width due to thermal expansion is 1.56 nm. Therefore, the thermal expansion of SU-8 is negligible. As shown in Table 1, our device exhibits a sensitivity comparable to that of a single-mode-based device, despite being based on the multi-mode waveguide. In addition, our device has a significant advantage in its simple fabrication process, enabling easier mass production and large tolerance to fabrication errors such as sidewall roughness or width mismatch of the waveguide.

Optics EXPRESS

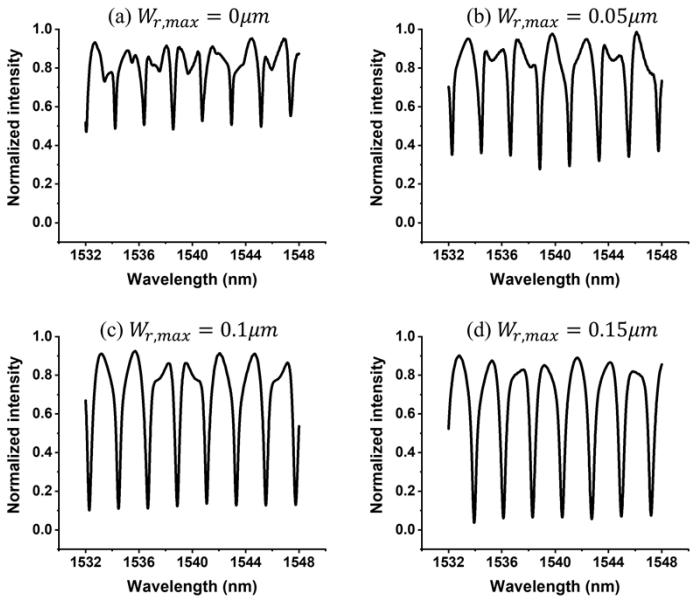

Fig. 10. Simulation results about resonance spectra based on 3 μm width waveguide according to the sidewall roughness (W_r) which is less than $W_{r,max}$.

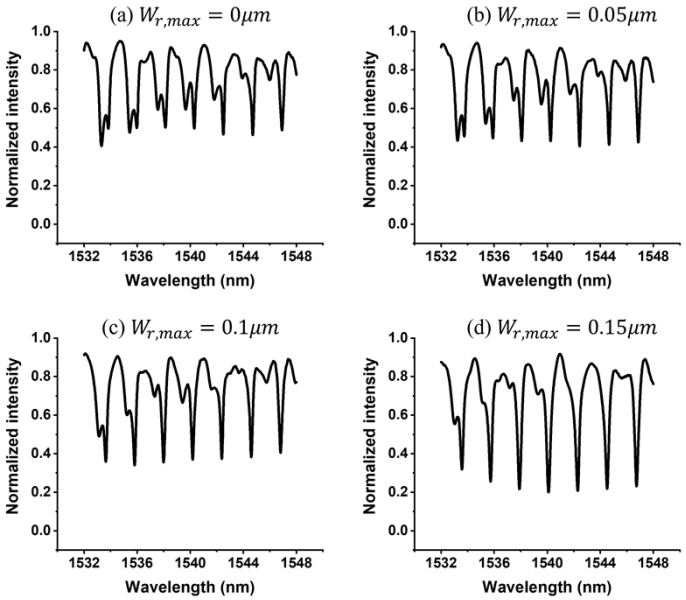

Fig. 11. Simulation results about resonance spectra based on 3.2 μm width waveguide according to the sidewall roughness (W_r) which is less than $W_{r,max}$.

Optics EXPRESS

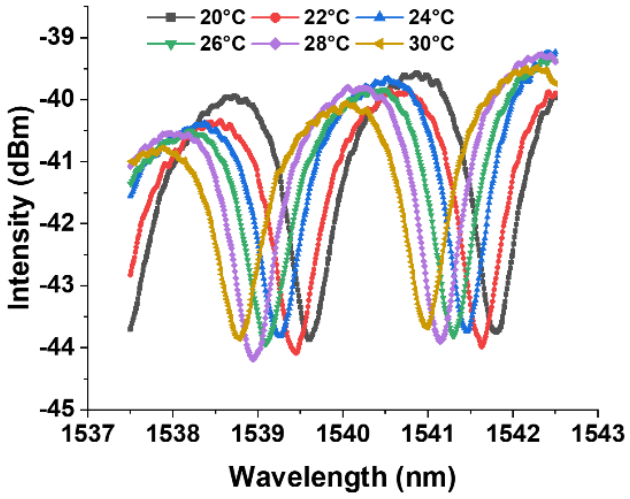

Fig. 12. Measured transmission spectra according to the temperature at intervals of 2°C.

Table 1. Performance comparison with other studies

Reference	Structure type	Wavelength (nm)	Refractive index range	Sensitivity (nm/RIU)	Sensitivity (pm/°C)
[2]	Surface plasmonic resonance	1100–1500	1.20–1.40	561	137
[4]	Mach-Zehnder Interferometer	1535 - 1550	-	-	172
[5]	Mach-Zehnder Interferometer	1570–1600	1.31–1.35	18.18	73
[6]	Single-mode fiber	1525–1565	1.320–1.355	132	88
[8]	Ring resonator	800–1200	1.00–1.08	1125	-
[10]	Ring resonator	1545–1575	1.00–1.01	690	-
	This work	1537–1543	-	630.8	82

5. Conclusion

In this paper, we experimentally verified the multi-mode waveguide-based resonator and analyzed the effect of sidewall roughness and waveguide widths. We performed simulations under various conditions to analyze the impact of the sidewall roughness on the mode discrimination. As a result, interestingly, the sidewall roughness accelerated the mode discrimination and suppressed the higher-order modes. Additionally, mode discrimination can be induced more efficiently in a narrow waveguide because the higher-order mode confinement factors decrease as the width of the waveguide becomes narrow. We simulated various resonators to analyze the effects of sidewall roughness and waveguide widths on the resonator. To demonstrate the sensor capabilities of the proposed resonator, we conducted the temperature variation experiment, yielding an average resonance shift was 82 pm/°C and the sensitivity of the resonator was 630.8 nm/RIU, which is comparable to that of a single-mode waveguide-based resonator. The proposed multi-mode resonator applied mode discrimination offers a remarkable advantage of simple fabrication, enabling mass production and large fabrication tolerance.

Funding. National Research Foundation of Korea (NRF-2023R1A2C100332, NRF-R1D1A1B07048145); Korea Institute for Advancement of Technology (P0017011).

Disclosures. The authors declare no potential conflicts of interest.

Optics EXPRESS

Data availability. Data underlying the results presented in this paper are not publicly available at this time but may be obtained from the authors upon reasonable request.

References

1. T. Duque, A. C. Chaves Ribeiro, H. S. de Camargo, P. A. da Costa Filho, H. P. Mesquita Cavalcante, and D. Lopes, "New Insights on Optical Biosensors: Techniques, Construction and Application," in *State of the Art in Biosensors - General Aspects* (InTech, 2013).
2. S. Weng, L. Pei, C. Liu, J. Wang, J. Li, and T. Ning, "Double-Side Polished Fiber SPR Sensor for Simultaneous Temperature and Refractive Index Measurement," IEEE Photonics Technol. Lett. **28**(18), 1916–1919 (2016).
3. B. Sun, Y. Wang, J. Qu, C. Liao, G. Yin, J. He, J. Zhou, J. Tang, S. Liu, Z. Li, and Y. Liu, "Simultaneous measurement of pressure and temperature by employing Fabry-Perot interferometer based on pendant polymer droplet," Opt. Express **23**(3), 1906 (2015).
4. X. Guan, X. Wang, and L. H. Frandsen, "Optical temperature sensor with enhanced sensitivity by employing hybrid waveguides in a silicon Mach-Zehnder interferometer," Opt. Express **24**(15), 16349 (2016).
5. T. Jiao, H. Meng, S. Deng, S. Liu, X. Wang, Z. Wei, F. Wang, C. Tan, and X. Huang, "Simultaneous measurement of refractive index and temperature using a Mach-Zehnder interferometer with forward core-cladding-core recoupling," Opt. Laser Technol. **111**, 612–615 (2019).
6. N. Zhang, W. Xu, S. You, C. Yu, C. Yu, B. Dong, and K. Li, "Simultaneous measurement of refractive index, strain and temperature using a tapered structure based on SMF," Opt. Commun. **410**, 70–74 (2018).
7. D. M. Elsheakh, M. I. Ahmed, G. M. Elashry, S. M. Moghannem, H. A. Elsadek, W. N. Elmazny, N. H. Alieldin, and E. A. Abdallah, "Rapid detection of coronavirus (Covid-19) using microwave immunosensor cavity resonator," Sensors **21**(21), 7021 (2021).
8. Y. Tang, Z. Zhang, R. Wang, Z. Hai, C. Xue, W. Zhang, and S. Yan, "Refractive index sensor based on fano resonances in metal-insulator-metal waveguides coupled with resonators," Sensors **17**(4), 784 (2017).
9. H. Han, B. Xiang, and J. Zhang, "Simulation and analysis of single-mode microring resonators in lithium niobate thin films," Crystals **8**(9), 342 (2018).
10. M. A. Butt, S. N. Khonina, and N. L. Kazanskiy, "Highly sensitive refractive index sensor based on hybrid plasmonic waveguide microring resonator," Waves in Random and Complex Media **30**(2), 292–299 (2020).
11. S.-H. Kim, D. Kim, S.-J. Jeon, E. Kim, J.-S. Lee, and Y.-W. Choi, "Analysis of regular polygonal ring resonator based on multi-mode waveguide," in *Proceedings of SPIE* (SPIE-Intl Soc Optical Eng, 2019), pp. 109211L1–109211L6.
12. D. H. Kim, S. J. Jeon, J. S. Lee, S. H. Hong, and Y. W. Choi, "Novel S-Bend Resonator Based on a Multi-Mode Waveguide with Mode Discrimination for a Refractive Index Sensor," Sensors **19**(16), 3600 (2019).
13. Y. J. Kim, S. H. Hong, J. S. Lee, S. J. Jeon, W. J. Choi, and Y. W. Choi, "Thermal Reflow Effect in Multi-Mode Waveguide of S-Bend Resonator With Mode Discrimination," IEEE Photonics J. **14**(1), 1–6 (2022).
14. E. A. J. Marcatili, "Dielectric Rectangular Waveguide and Directional Coupler for Integrated Optics," The Bell Syst. Tech. J. **48**(7), 2071–2102 (1969).
15. G. B. Hocker and W. K. Burns, "Mode dispersion in diffused channel waveguides by the effective index method," Appl. Opt. **16**(1), 113–118 (1977).
16. Y. A. Vlasov and S. J. Mcnab, "Losses in single-mode silicon-on-insulator strip waveguides and bends," Opt. Express **12**(8), 1622–1631 (2004).
17. M. Eryürek, Z. Tasdemir, Y. Karadag, S. Anand, N. Kilinc, B. E. Alaca, and A. Kiraz, "Integrated humidity sensor based on SU-8 polymer microdisk microresonator," Sens. Actuators, B **242**, 1115–1120 (2017).
18. D. Dai, L. Yang, Z. Sheng, B. Yang, and S. He, "Compact microring resonator with 2 × 2 tapered multimode interference couplers," J. Lightwave Technol. **27**(21), 4878–4883 (2009).
19. M. Ibrahim, J. H. Schmid, and A. Aleali, *et al.*, "Athermal silicon waveguides with bridged subwavelength gratings for TE and TM polarizations," Opt. Express **18**(19), 20251–20262 (2010).